Intelligent Automation & Soft Computing

Tech Science Press

DOI: 10.32604/iasc.2023.035392
Article

Fluid Flow and Mixed Heat Transfer in a Horizontal Channel with an Open Cavity and Wavy Wall

Tohid Adibi[1], Shams Forruque Ahmed[2,*], Omid Adibi[3], Hassan Athari[4], Irfan Anjum Badruddin[5] and Syed Javed[5]

[1]Department of Mechanical Engineering, University of Bonab, Bonab, Iran
[2]Science and Math Program, Asian University for Women, Chattogram, Bangladesh
[3]Energy Management Group, Energy and Environment Research Center, Niroo Research Institute, Tehran, Iran
[4]Department of Mechanical Engineering, Elm-o-Fann University College of Science and Technology, Urmia, Iran
[5]Mechanical Engineering Department, College of Engineering, King Khalid University, Abha, 61421, Saudi Arabia
*Corresponding Author: Shams Forruque Ahmed. Email: shams.f.ahmed@gmail.com
Received: 19 August 2022; Accepted: 23 November 2022

Abstract: Heat exchangers are utilized extensively in different industries and technologies. Consequently, optimizing heat exchangers has been a major concern among researchers. Although various studies have been conducted to improve the heat transfer rate, the use of a wavy wall in the presence of different types of heat transfer mechanisms has not been investigated. This study thus investigates the mixed heat transmission behavior of fluid in a horizontal channel with a cavity and a hot, wavy wall. The fluid flow in the channel is considered laminar, and the governing equations including continuity, momentum, and energy are all solved numerically. The numerical solution is stabilized by using a first-order multi-dimensional characteristic-based scheme in combination with a fifth-order Runge-Kutta method. The flow and heat transfer effects of varying Richardson numbers, Reynolds numbers, wave amplitude, wavelength, channel height, and cavity width are examined. The results indicate that the mean Nusselt number increases with an increase in Reynolds number, wave amplitude, and cavity width, while it decreases with an increase in Richardson number, wavelength, and channel height. The minimum Nusselt number is calculated to be 0.7, whereas the maximum Nusselt number is 27.09. The Nusselt number has only increased by 40% in the higher depths of the cavity, despite the Richardson number being 10,000 times larger. But this figure increases to 130% at lower depths. The mean Nusselt number is thus significantly influenced by channel height and cavity width. The influence of wave amplitude on the mean Nusselt number is twice that of wavelength.

Keywords: Mixed heat transfer; wavy wall; horizontal channel; open cavity; numerical simulation

1 Introduction

Free, forced, and mixed convective flow and heat transfer, due to their wide applications in industry, have been studied extensively by several researchers. For instance, Ali et al. [1] studied mixed convection numerically. The nano-fluid flow with an electromagnetic field was considered in their study to improve heat transfer rates. Yang et al. [2] reviewed the experimental and numerical researches conducted on mixed convection for non-newtonian fluids. The applied scheme was compared in these researches. In another work, mixed convection was studied numerically by Qaiser et al. [3]. A written code in MATLAB was used to simulate nano-fluid mixed convection. The heat transfer from cavities and channels is currently receiving noticeable attention from scientists because of their extensive engineering applications. Important applications of the channels are heat transfer rate enhancement in heat exchangers, cooling systems, air conditioning, refrigeration, gas turbine combustor, dryer machine, chemical mixer, nuclear reactors, internal combustion engines, aeroplane suction, industrial heater, rocket nozzle, compact heat exchanger, and centrifugal pump. Sadr et al. [4] numerically studied mixed convection in a cavity. The SIMPLE scheme was used for numerical simulations. Mixed convection in the cavity was the subject of other research that was performed by Nazari et al. [5]. The simulations were done numerically by written code in FORTRAN 95. Non-newtonian nano-fluid heat transfer simulations were performed in different Richardson numbers in this work. Salamai et al. and Eid et al. [6,7] proposed a new algorithm to solve mechanical problems. Taher et al. [8] studied the mixed convective flow of water in a horizontal channel under constant thermal flux and concluded that the Nusselt number for mixed convection results in a higher heat transfer coefficient than forced convection. Xiong et al. [9] simulated the mixed convective flow of a Newtonian fluid in a triangular cavity with adiabatic circular blocks at its right and left, and analyzed the effects of physical parameters such as Reynolds number, Hartman Number, Richardson number, and Nusselt number on the velocity and temperature contours. They found out that the heat transfer rate decreases with rising of the Hartman number. The effect of the Prandtl number on the mixed convective flow in a horizontal channel heated from the below surface was studied by Sahraoui et al. [10] using the thermal Boltzmann method, The Prandtl number significantly affected the flow and temperature field, and heat transfer increased in the range of $0.05 < Pr < 0.3$, while the Prandtl numbers higher than 0.3 had negligible effects.

Using waves and ribs on the wall that has been studied by researchers is one of the passive methods for enhancing heat transfer, which is based on increasing mixing, creating vortices, circulating motions, and increasing turbulence. Li et al. [11] performed a three-dimensional numerical work to survey the effect of helical-rib roughness on heat transfer rate. The mixed convection was simulated in different Grashof numbers in this work. Xie et al. [12] carried out a three-dimensional numerical study on mixed convection. The influence of rib on heat transfer rate was surveyed. The ribs were controlled dynamically in this work. Another three-dimensional numerical work was conducted by Razavi et al. [13]. The effect of different ribs and fins on Nusselt number was surveyed and the optimum shape of ribs and fins was proposed by the authors. The mixed convection in the heat exchanger was simulated in different Reynolds numbers. The channel with wavy walls is the other way to improve the heat transfer rate that the researcher worked on it. Tang et al. [14] analyzed heat transfer and pressure drop inside a channel with zigzag baffles. One of the most significant findings of the study was that a zigzag baffle with a rectangular section exhibited the highest efficiency compared to other baffle shapes. Yousefzadeh et al. [15] simulated the mixed convective heat transfer in a square cavity. In the considered geometry, the cold stream enters the cavity, which contains an isothermal heat source at its center. The authors reported that as Reynolds number increases, temperature gradients near the hot surface are reduced, velocity gradient and boundary layer expansion are amplified, and the

friction coefficient reaches its maximum value. This paper evaluated the fluid-heat behavior of airflow inside the open cavity in presence of a horizontal channel and geometrical changes in the bottom wall. Control parameters for the simulation focused on the geometrical and flow changes. Parameters that are considered for the wavy wall include the length and amplitude of the wall wave. In the channel and cavity, the height and width of the cavity change, and fluid flow experiences variations in Richardson and Reynolds numbers. Flow is laminar according to the variation range of the Reynolds number.

Ullah et al. [16] studied the heat energy transfer phenomenon of a rotating surface using a 3D water-based nanofluid. They considered the simultaneous effects of couple stress and thermal radiations. The velocity component experienced a decrease with increasing nanoparticle volume fraction and rotation parameter. Khan et al. [17] examined the hydrodynamic flow of an isotropic and incompressible Casson fluid via a yawed cylinder. When the Casson parameter, yaw angle, and convection parameter increased, the heat transfer rate, skin friction, and fluid velocity declined. Ullah et al. [18] analytically evaluated hydrothermal features of a laminar, incompressible, and unsteady nanofluid motion via a porous capillary. In their study, the hybrid nanofluid was synthesized by blending nanomaterials of zinc oxide and graphene oxide with blood acting as the host fluid. They showed that increasing the magnetic field strength led to an enhancement of fluid friction. Hussain et al. [19] combined the Daftardar–Jeffery polynomials with the optimal homotopy asymptotic method to solve the generalized Hirota–Satsuma coupled system of Korteweg–de Vries equations. The results revealed that it was a more explicit, reliable, and efficient analytical technique. Concerning radiation, heat source, and variable magnetic field, Rizk et al. [20] studied the heat transfer phenomenon during hybrid nanofluid migration. The temperature of the fluid was enhanced in the study by increasing the Eckert number, heat source strength, nanomaterial concentrations, non-steadiness, and radiation parameters. Considering the influence of mass transfer, thermal radiation, and Hall current, Khan et al. [21] examined the 3D Carreau fluid stream via a stretching and porous sheet. The concentration field was found to grow with the Soret number and decrease with the Schmidt number.

In a study by Alharbi et al. [22], the hydrothermal features of a 3D nonlinear Carreau fluid motion over a revolution's paraboloid surface were analyzed. They demonstrated that the convective heat transfer can be improved by enhancing the Brownian motion. Arifeen et al. [23] presented a numerical study for the solutions of higher-order linear and nonlinear boundary value problems. In nonlinear cases, quasilinearization was applied to deal with nonlinearity. It was deduced that increasing the resolution level improves precision. Bilal et al. [24] studied the computational and theoretical aspects of thermal analysis of Sutterby fluid encompassing radiation characteristics over a linearly moving sheet implanted in a stratified medium. They concluded that concentration distribution increases with the magnitude of the solutal stratification parameter. Bilal et al. [25] analyzed the thermal features of Carreau liquid flowing on variably thickened non-uniformly rotating disk. It was reported that radially and tangentially directed wall drag reduces with increasing magnitude of the power-law exponent index. Akbar Qureshi et al. [26] carried out a numerical study to show the flow behavior of non-Newtonian fluid via orthogonal porous surfaces. Higher boundary layer thicknesses in the presence of single-wall carbon nanotubes contributed to the increased heat transfer rate. The quality of a water-based hybrid nano liquid stream with scattering of single-wall carbon nanotubes was recently discussed by Shah et al. [27], who used a thermal conductance model that comprises the characteristics of nanolayer formation, particle size, and shape. The thermal conductance of the base fluid was improved as the particle radius and nanolayer thickness increased. Microchannels with optimal thermal performance were achieved by Shah et al. [28] by utilizing a triangular cavity with varying aspect ratios. To prevent excessive energy loss in heat exchangers and micro heat sinks, a cold cylinder was installed within a triangular enclosure. As reported by the authors, the Rayleigh number

increased local heat transfer coefficients and kinetic energy. Shah et al. [29] investigated the double diffusive natural convection regime for the Casson fluid flow. They also measured kinetic energy and other important terms relative to dimensionless involved parameters.

In order to improve heat transfer, the sinusoidal channel is one of the channels that has minimal effect on the pressure drop along the length of the channel. However, in the previous studies, the mixed convection with a wide range of Reynolds and Richardson numbers in a channel with a sinusoidal channel has not been studied. The mixed convection with a wide range of Reynolds and Richardson numbers in a channel with a sinusoidal channel has been studied in this work for the first time. In each wave of a sinusoidal channel, a very complex flow is formed that proceeds with high intensity. The other novelty of the present work is using a novel multi-dimensional characteristics-based scheme. In this scheme, artificial wave propagation is considered. This scheme is based on compressible flow schemes, and in incompressible flows, artificial waves propagate at pseudo sound speed. This method has superior convergence speed and stability compared to other schemes for incompressible flows. Effects of changes in Richardson number, Reynolds number, wave amplitude, wavelength, channel height, and cavity width on flow and heat transfer are also assessed and discussed. The outcomes of the present study will help mechanical engineers and heat exchanger designers in achieving the optimal design of systems containing a channel and an open cavity. The HVAC industry could use the findings to enhance the performance of its systems.

2 Governing Equations of Flow and Numerical Methods

In the present research, two-dimensional, laminar, and steady flow is considered. The Boussinesq approximation is employed in the momentum equation to account for the density variations. Continuity (Eq. (1)), momentum in two directions (Eqs. (2) and (3)), and energy (Eq. (4)) equations are as follows [30].

$$\frac{\partial u}{\partial x}+\frac{\partial v}{\partial y}=0. \tag{1}$$

$$\rho\left(\frac{\partial u}{\partial t}+u\frac{\partial u}{\partial x}+v\frac{\partial u}{\partial y}\right)=-\frac{\partial p}{\partial x}+\mu\left(\frac{\partial^2 u}{\partial x^2}+\frac{\partial^2 u}{\partial y^2}\right). \tag{2}$$

$$\rho\left(\frac{\partial v}{\partial t}+u\frac{\partial v}{\partial x}+v\frac{\partial v}{\partial y}\right)=-\frac{\partial p}{\partial y}-\beta\rho\left(T_c-T\right)g+\mu\left(\frac{\partial^2 v}{\partial x^2}+\frac{\partial^2 v}{\partial y^2}\right). \tag{3}$$

$$\rho c_p\left(\frac{\partial T}{\partial t}+u\frac{\partial T}{\partial x}+v\frac{\partial T}{\partial y}\right)=k\left(\frac{\partial^2 T}{\partial x^2}+\frac{\partial^2 T}{\partial y^2}\right). \tag{4}$$

The governing equations of the flow can be written as follows [30].

$$\frac{\partial}{\partial t}(\rho\phi)+\left(\frac{\partial}{\partial x_i}\right)(\rho u_i\phi)=\left(\frac{\partial}{\partial x_i}\right)\left(\Gamma\frac{\partial\phi}{\partial x_i}\right)+S_\phi \tag{5}$$

where ϕ is a physical variable like temperature. In the above equation, Γ is the diffusion coefficient and S is the source term. Table 1 represents the governing value of the flow in the general form.

The following non-dimensional variables are used to non-dimensionalize the governing equations:

$$X=\frac{x}{H},\ Y=\frac{y}{H},\ U=\frac{u}{u_c},\ v=\frac{v}{u_c},\ P=\frac{P}{\rho {u_c}^2},\ \theta=\frac{T-T_c}{T_h-T_c},\ \tau=\frac{u_c t}{H}. \tag{6}$$

Table 1: Different parts of governing equations of flow

Equation	ϕ	Γ	S_ϕ
Continuity	1	0	0
X-momentum	u	μ	$-\frac{\partial p}{\partial x}$
Y-momentum	v	μ	$-\frac{\partial p}{\partial y}-\beta\rho\left(T_c-T\right)g$
Energy	T	$\frac{k}{C_p}$	0

In these relations, H is the characteristic length and u_c is the reference velocity (inlet velocity). The non-dimensional forms of the governing equations are as follows.

$$\frac{\partial U}{\partial X}+\frac{\partial V}{\partial Y}=0 \tag{7}$$

$$\frac{\partial U}{\partial \tau}+U\frac{\partial U}{\partial X}+V\frac{\partial U}{\partial Y}=-\frac{\partial P}{\partial X}+\frac{1}{\mathrm{Re}}\left(\frac{\partial^2 U}{\partial X^2}+\frac{\partial^2 U}{\partial Y^2}\right) \tag{8}$$

$$\frac{\partial V}{\partial \tau}+U\frac{\partial V}{\partial X}+V\frac{\partial V}{\partial Y}=-\frac{\partial P}{\partial Y}+\frac{1}{\mathrm{Re}}\left(\frac{\partial^2 V}{\partial X^2}+\frac{\partial^2 V}{\partial Y^2}\right)+\frac{Gr}{\mathrm{Re}^2}\theta \tag{9}$$

$$\frac{\partial \theta}{\partial \tau}+U\frac{\partial \theta}{\partial X}+V\frac{\partial \theta}{\partial Y}=\frac{1}{\mathrm{Re.\,Pr}}\left(\frac{\partial^2 \theta}{\partial X^2}+\frac{\partial^2 \theta}{\partial Y^2}\right) \tag{10}$$

The non-dimensional numbers in the above equations, i.e., Reynolds number, Grashof number, and Prandtl number, are defined as the following. Richardson number is defined as a combination of Grashof and Reynolds numbers as in Eq. (5) to determine the type of convection.

$$\mathrm{Re}=\frac{v_0 L}{\nu},\ Gr=\frac{g\beta L^3(T_h-T_c)}{\nu^2},\ \mathrm{Pr}=\frac{C_P\mu}{k},\ Ri=\frac{Gr}{\mathrm{Re}^2}. \tag{11}$$

Reynolds number represents forced convection and Grashof number represents natural convection. Therefore, the Richardson number denotes the interaction of natural and forced convective flows. In other words, when simultaneous effects of forced and free convection exist the Richardson number is in the order of unity. When the Richardson number is much lower than one effect of forced convection is dominant and if the Richardson number is much larger than one the convection is natural and forced convection is negligible. In this section of the paper, the geometry of the boundary value problem is described in detail. The sinusoidal wave of the wall is as in Eq. (12).

$$y=-\frac{\mathrm{H}}{2}-\mathrm{ASIN}\left[(\mathrm{x}-\mathrm{L}_1)\frac{2\pi}{\mathrm{L}_\mathrm{w}}\right]\ \mathrm{L}_1\le \mathrm{x}\le \mathrm{L}_2 \tag{12}$$

where the geometrical parameters include H the channel height, L_1 inlet length, L_2 inlet length to the end of the wave, and L_w distance between peaks of two waves. The amplitude and length of the wave

in the channel are non-dimensionalized by using the half of height of the channel as follows:

$$\lambda = \frac{L_w}{H/2}\ \alpha = \frac{a}{H/2} \tag{13}$$

Boundary conditions of the problem at the inlet, sidewall, bottom wavy wall, and outlet are given in Table 2.

Table 2: Boundary conditions of the simulated physical problem

Boundary	Applied boundary condition
Channel inlet	$u = U_{in},\ v = 0,\ T = T_{in} = 293.15$ K
Channel outlet	$P = P_{atm}$
Top insulated wall	$u = v = 0,\ \partial T/\partial y = 0$
Wavy wall	$u = v = 0,\ T = T_w = 333.15$ K

To find the boundary conditions in numerical simulation, second-order extrapolation is employed. Thus, velocities at the outlet and pressure at the inlet and on the solid boundaries are determined using this method. The non-dimensional Nusselt number is defined as Eq. (14), which is expressed for the hot wavy wall [30].

$$Nu = \frac{hL}{k} = \frac{\left[\frac{q''}{(T_h - T_c)}\right]L}{k} \tag{14}$$

In the above equation, k is the fluid thermal conductivity, h is the local convection coefficient, and q'' is the heat transfer rate on the hot surface. According to Fourier law, the heat transfer rate from the hot wall can be calculated as follows:

$$q'' = -k\frac{\partial T}{\partial y}_{y=o} \tag{15}$$

Local Nusselt number on the hot wall can be predicted from non-dimensional parameters as the following [30].

$$Nu = -L\frac{1}{T_h - T_c}\frac{\partial T}{\partial y}_{y=o} = -L\frac{\partial \theta}{\partial y}_{y=o} = \frac{\partial \theta}{\partial Y}_{y=o} \tag{16}$$

The average Nusselt number can be written as follows by integrating it on the wall [30]:

$$Nu = \frac{1}{l_1}\int_{l_1}^{0}\frac{\partial \theta}{\partial Y}_{y=o} dX \tag{17}$$

where l_1 is the non-dimensional length of the hot wall. To describe and draw the streamlines, the stream function is defined as below, which is the relationship between stream function and mass conservation and has the following relationship with velocity:

$$u = \frac{\partial \psi}{\partial y},\ v = -\frac{\partial \psi}{\partial x} \tag{18}$$

In this study, the focus is on mixed forced and free convection in a horizontal channel with an open cavity in the middle part of the bottom wall. The bottom wall geometry is wavy. The sidewalls of the cavity are cold and the bottom wall is considered hot and with a sinusoidal wavy shape. The location of

the hot, cold, and wavy walls with the boundary conditions are illustrated in Fig. 1. The flow is laminar and the main innovation of the research is on variations of various parameters such as Richardson number, Reynolds number, wave amplitude, wavelength, cavity length, and cavity width. For numerical solutions, an upwind scheme that is developed for two-dimensional incompressible flows is applied. Time marching is performed using the Runge-Kutta method to accelerate the convergence rate In addition, viscous terms are calculated using second-order averaging on the secondary cell [31]. For more clarity, the flowchart of this work is shown in Fig. 2.

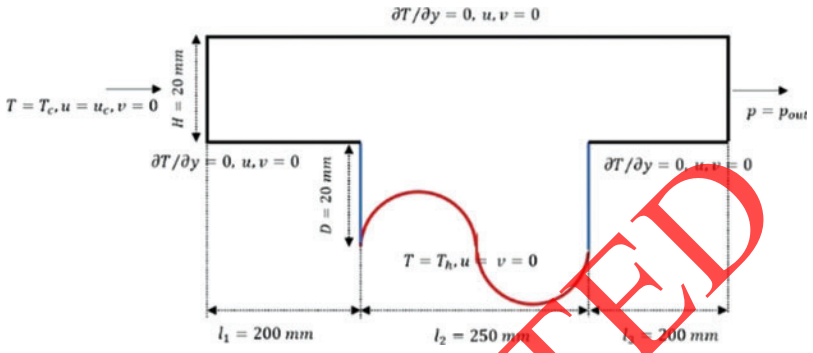

Figure 1: Schematic of the channel and open cavity with a wavy wall, boundary conditions, and dimensions

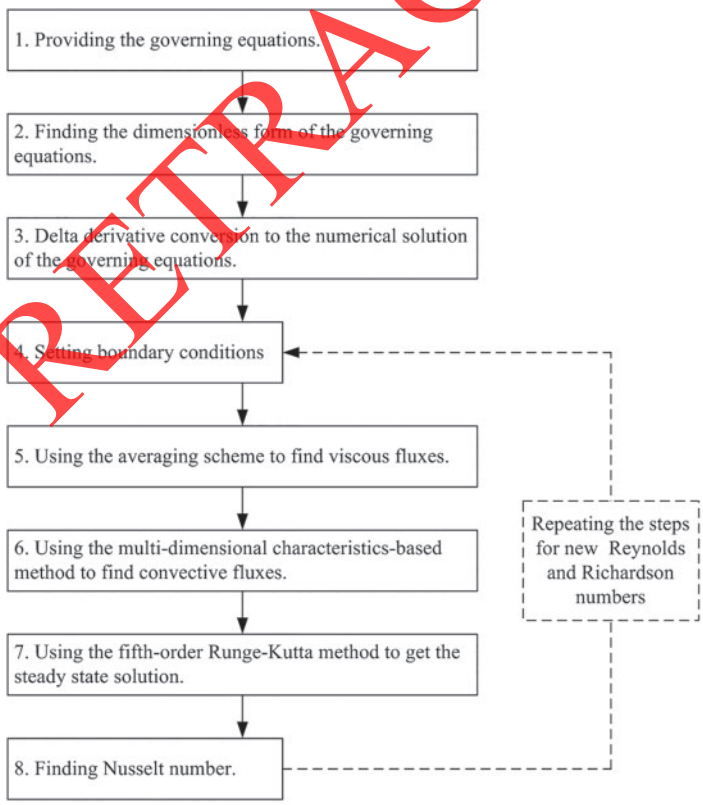

Figure 2: Flowchart of current work

Different cases of simulation and problem variables, which include Richardson number (Ri), cavity length (L), cavity depth (D), wave amplitude (A), and Reynolds number (Re), are given in Table 3. It should be mentioned that the Reynolds number is calculated based on the inlet length of the channel, and the length and amplitude of the wave are non-dimensionalized with channel height.

Table 3: Different cases of simulation with changing the parameters

Cases	Variables	Range of variations
1	*Ri*	0.1, 1, 10, 100
2	*L*	50, 150, 250 mm
3	*D*	10, 30, 50 mm
4	*A*	4, 7, 10 mm
5	λ	0.10, 0.15, 0.20 mm
6	*Re*	10, 100, 1000

Grid independence is crucial for every numerical research. Computation time and stability of analysis face challenges with increasing the cell numbers, therefore, choosing the optimum grid is important. In Fig. 3a, the variation of the average Nusselt number in different grids is shown. In Fig. 3a, the Richardson number is 10 and the length and height of the channel are fixed. The figure shows that the 113565 cells are suitable for the simulation and there is no need to increase the cell numbers to 224534 since the average Nusselt number becomes almost constant. The clustered tetrahedron grid is used for numerical simulations. The clustering factor is 1.05 in this work. Clustering is done near the solid borders to have better accuracy in simulations. The convergence criterion for simulation is considered 10^{-6}. This magnitude provides enough accuracy for engineering applications. The validation is done for more confidence in this convergence criterion. Nonlinear governing equations are solved by a characteristics-based scheme. Different works demonstrate the accuracy and stability of this work. This method is more stable than the usual method such as averaging method [30,31]. Another comparison is performed in the present work with the results of Manca et al. and is shown in Fig. 4. Validation is performed by comparing the results with similar works by Manca et al. [32]. They studied experimentally the fluid flow inside a channel with an open cavity and vertical hot wall. In their simulation, they addressed the changes in the Reynolds and Richarson numbers, and the Reynolds number was assumed in the range of 1000 to 8700, and the Richardson number was considered between 30 and 110. The assumptions for the fluid flow were laminar, Newtonian, incompressible, and two-dimensional flow. Variation of the average Nusselt number by changing the cavity length at different Richardson numbers is shown in Fig. 3b, where the numerical results are compared with experimental data by Manca et al. [32].

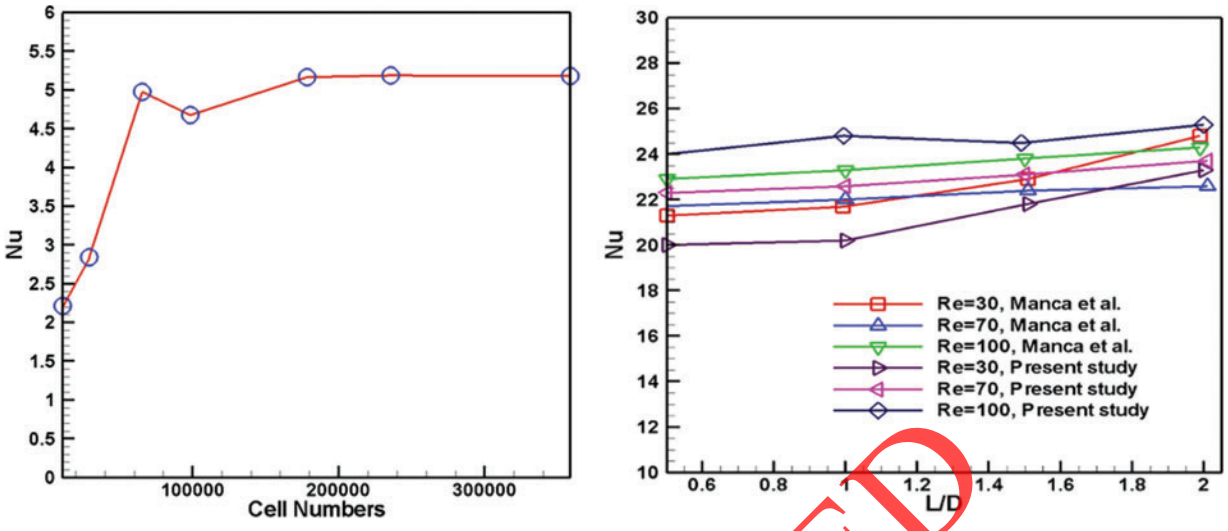

Figure 3: (a) Variations of average Nusselt number in different grids to survey grid independence. (b) Comparison between the variation of the average Nusselt number and the study by Manca et al. [32] (Re = 1000, H/D = 1.0)

3 Results and Discussion

The sinusoidal channel is one of the channels that enhance the heat transfer while having little effect on the pressure drop along the channel length. The mixed convection with a wide range of Reynolds and Richardson numbers in a channel with a sinusoidal channel has been studied in this work for the first time. Effects of changes in Richardson number, Reynolds number, wave amplitude, wavelength, channel height, and cavity width on flow and heat transfer are also assessed and discussed. The output of this research assists to obtain the optimum design of the systems that include a channel and an open cavity. In other words, the results of this study are useful for mechanical engineers and designers of heat exchangers. HVAC industries could use the results of this research to improve the performance of their systems. In this section, changes in the depth of the cavity are analyzed for three cases shallow, medium-depth, and deep, and two minimum and maximum wave amplitudes are considered for this case. In this simulation $Ri = 0.1$ and $Gr = 10^3$. The obtained streamlines and temperature contours are obtained which are depicted in Fig. 4.

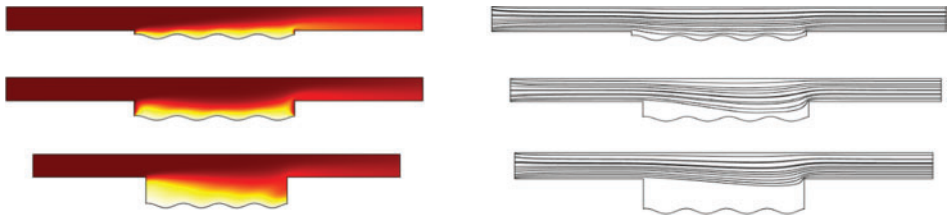

Figure 4: Streamlines (right) and temperature contours (left) for different depths of the cavity at constant amplitude

As seen in Fig. 4, the penetration of the fluid flow into the cavity decreases by increasing the cavity depth, so it is expected that heat transfer from the hot wall to the cavity outlet reduces, which is evident

from the temperature contours. In Fig. 5a, variations of the average Nusselt number with increasing depth at different amplitudes are illustrated. Fig. 5a shows that the deeper the cavity is smaller the heat transfer from the hot surface becomes, which is shown by a decrease in the average Nusselt number. In addition, by increasing the wave amplitude heat transfer from hot surfaces enhances. The increment is negligible for the deep cavity since the velocity of flow inside the cavity is small. As the depth of the cavity increases, the Nusselt number is reduced. For larger depths, the reduction of the Nusselt number is more severe. The influence of amplitude on the Nusslet number is less than the influence of cavity depth. Fig. 5b shows that the increase in the depth of the cavity decreases the horizontal velocity along the central axis, and at the small depths of the cavity increasing the amplitude leads to a rise in horizontal velocity in the cavity, while at the depths larger than 10 amplitude does not affect the velocity significantly. The change in the depth of the cavity and the change in the amplitude causes complex changes in the velocity profile. The velocity of the boundary layer decreases rapidly in close-walled regions. Fluid particles move toward the center, thus increasing mass flow and velocity at intermediate levels occur.

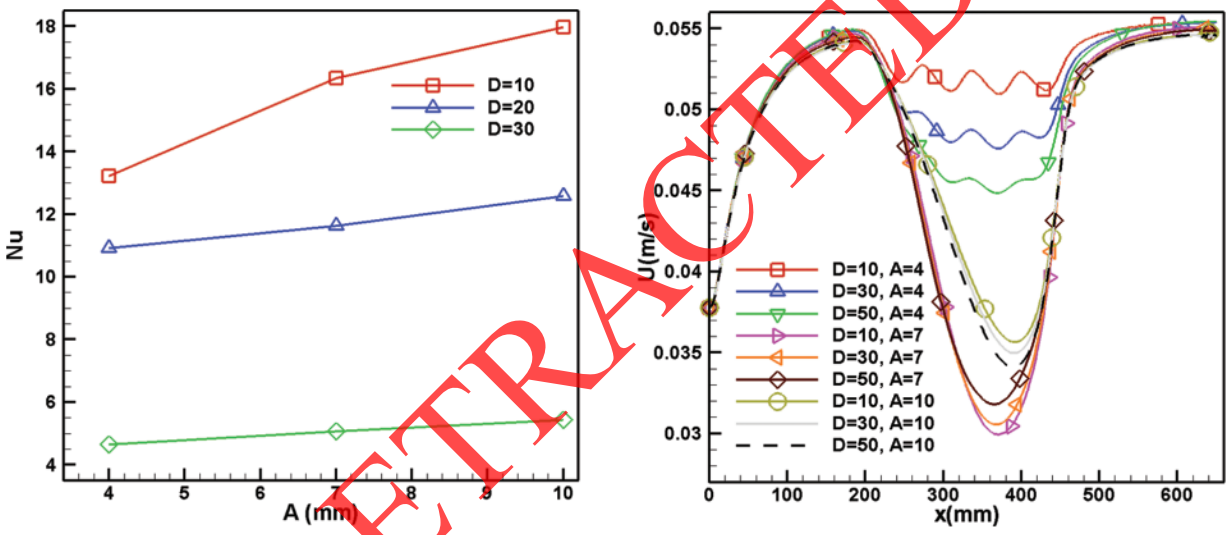

Figure 5: (a) Variations of the average Nusselt number with increasing the amplitude and depth of the cavity (b) Variations of horizontal velocity on the horizontal central axis with changes in the depth and amplitude of the function

The Reynolds number and the channel width are both variables in this section. Reynolds number varies in the range of laminar flow with values of 10, 100, and 1000, and the width of the channel changes between three values of a small, medium, and large width. It is expected that flow behavior in narrow channels appears as incomplete penetration of fluid into the cavity and increasing the Reynolds number increases the flow velocity inside the cavity, which can affect the heat transfer too. Results for variations of the average Nusselt number at different Reynolds numbers and widths are shown in Fig. 6.

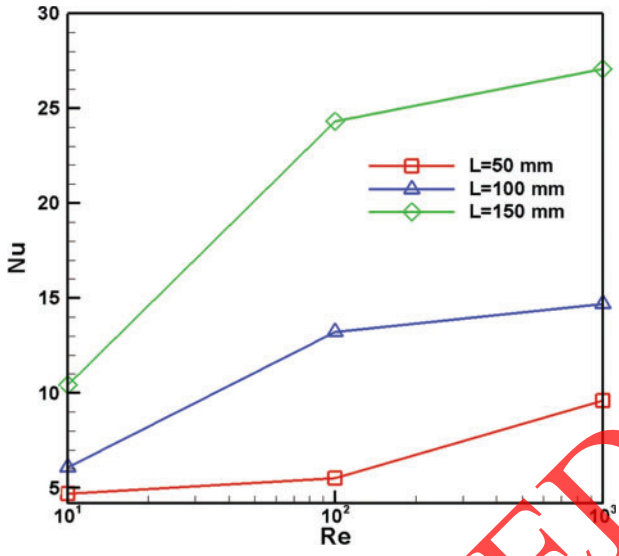

Figure 6: Average Nusselt number with increasing the Reynolds number and length of the cavity

Increasing the Reynolds number results in a decrease in the average Nusselt number, and in addition, at different Reynolds numbers, an increase in the length rises the average Nusselt number, which can be seen in Fig. 6. The Nusselt number multiplies by three as the length multiplies by three. The heat transfer rate is also increased by a factor of three in this configuration. Therefore, this technique has the potential to be an effective means of enhancing heat transfer. But the potential costs of this approach need to be taken into account. The main drawback of this approach is the cost of increasing the heat transfer rate. The goal of this section is to alter the length and amplitude of the wave at constant flow characteristics. In this section, the cavity is assumed at its deepest, and the length of the cavity is at its maximum value. Therefore, different simulation cases are formed by changing the length and amplitude of the wave. It is expected that the flow path and heat transfer change significantly at the large length and amplitude of the wave. In Fig. 7, contours of pressure and velocity are depicted changing the length and wave at constant Richardson of $Ri = 10$ and Grashof of $Gr = 10^3$. Paying attention to Fig. 7 demonstrates that at low Reynolds numbers, flow inside the channel with a deep cavity does not change with geometry variations, and increasing the wavelength does not affect the flow path. In Fig. 8a, variations of the average Nusselt number with increasing the length and amplitude of the wave are shown.

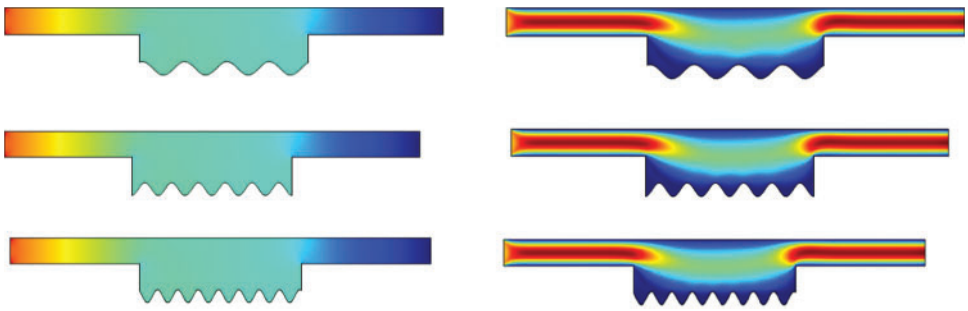

Figure 7: Velocity contours (right) and pressure contours (left) with changes in the wavelength at constant amplitude

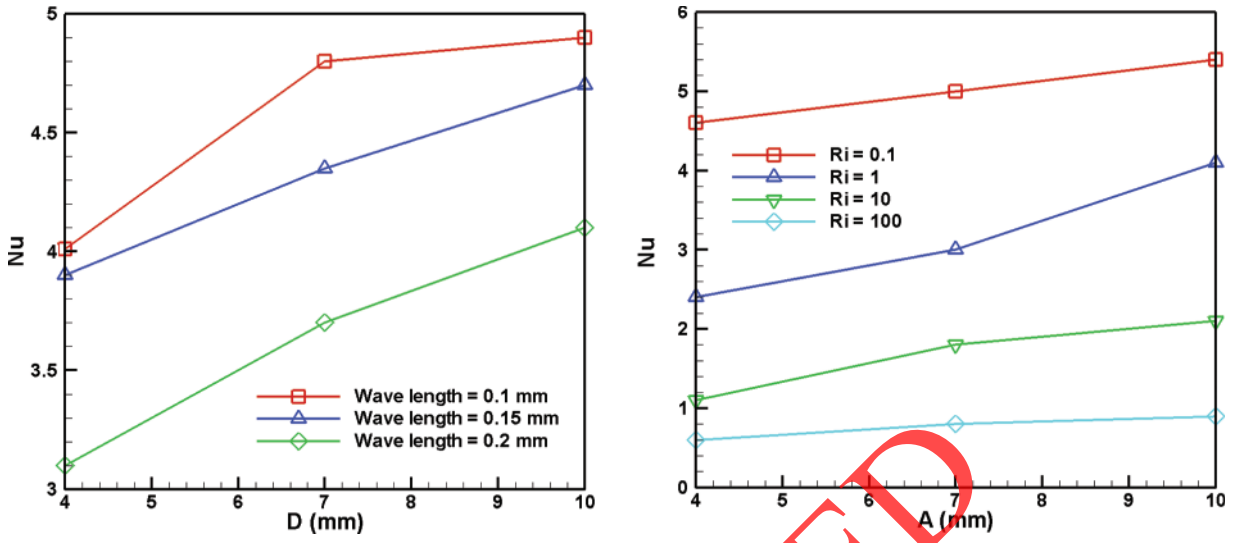

Figure 8: (a) Variations of the average Nusselt number with wavelength and amplitude (b) Variations of the Nusselt number with changes in the richardson number and amplitude

Fig. 8a shows that at low Reynolds numbers, with increasing the number of waves Nusselt number decreases and at any wavelength increasing the amplitude rises the average Nusselt number. In this section of results, changes in Richardson number are simulated for four cases by changing the wave amplitude at three values. In this case, the depth of the cavity is maximum so the effects of the free convection are more evident. Variations of the average Nusselt number with wave amplitude and Richardson number are shown in Fig. 8b.

According to Fig. 8b, it can be concluded that increasing the Richardson number increases the effects of free convection in heat transfer and decreases the effect of forced convective heat transfer; therefore, at high Richardson numbers increasing the wave amplitude does not significantly influence the heat transfer and the average Nusselt number in the cavity. However, at low Richardson numbers, it enhances the heat transfer from the wavy surface. In this section, the wavelength is varied at different Richardson numbers so the contributions of free and forced convective heat transfer are determined at all the wavelengths. Streamlines and isotherms in Fig. 9 show the flow pattern and heat transfer at a different wavelength and Richardson number of $Ri = 100$. It can be observed from this figure that the dominant mechanism of heat transfer at different wavelengths is free convection, and the location of the central vortex does not change with the wall wavelength, therefore heat transfer rate with increasing the wavelength at maximum Richardson does not vary significantly, which is evident in the temperature contours. Variations of the average Nusselt number with changes in the wavelength are shown in Fig. 10, where the second variable is the Richardson number and the depth and wave amplitude are constant. The figure demonstrates that increasing the Richardson number and decreasing the contribution of forced convective heat transfer leads to a decline in the average Nusselt number, which occurs at all wavelengths. In addition, increasing the wavelength at constant Richardson number results in a decrement in heat transfer and the average Nusselt number.

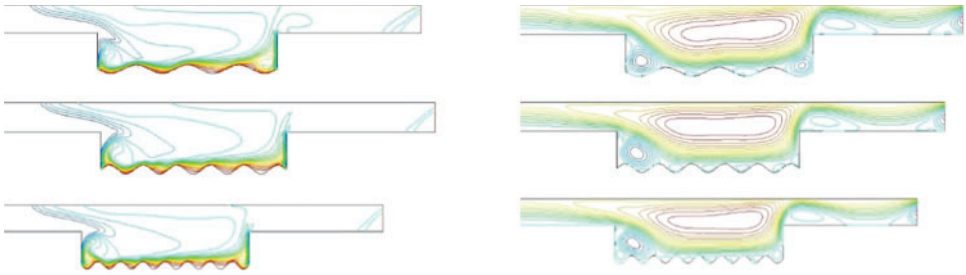

Figure 9: Streamlines and isotherms in different wall wavelengths at the maximum Richardson

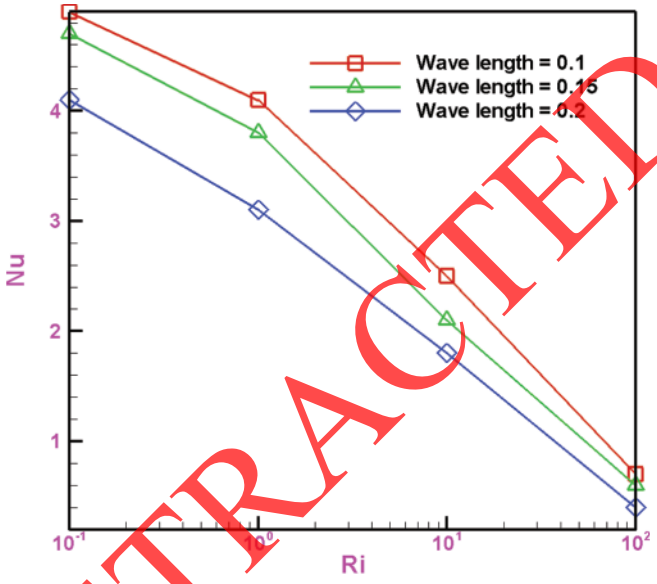

Figure 10: Variations of the average Nusselt number with increasing the Richardson number at different wavelengths

In this section, variations of the Richardson number with increasing the depth of the cavity are studied. Streamlines and isotherms in Fig. 11 show the changing trends at different depths and Richardson number of 10. In this case, the amplitude and length of waves are fixed. As seen in the figure, it can be deduced that at high Richardson numbers an increase in depth of the cavity leads to the formation of vortices in the cavity, which are the main factors of heat transfer, while it does not happen at low Richarson numbers where the forced convective heat transfer is the dominant mechanism. Variations of the average Nusselt number at different Richardson numbers and depths of the cavity are presented in Fig. 12. It shows that increasing the Richardson number and rising of free convection heat transfer and vortex inside the cavity leads to a decline in the average Nusselt number, and with increasing the depth at low Richardson numbers the heat transfer increases. However, at high Richardson numbers changes in the average Nusselt number is smaller. The fluid velocity in the cavity decreases as the depth of the fluid velocity increases. The heat transfer rate between the solid wall and the fluid decreases as the fluid velocity decreases. As a result, The convective coefficient and the Nusselt number are reduced. Despite 10,000 times the Richardson number, the Nusselt number has only increased by 40% at higher depths of the hole. At shallower depths, however, this number increases to 130%.

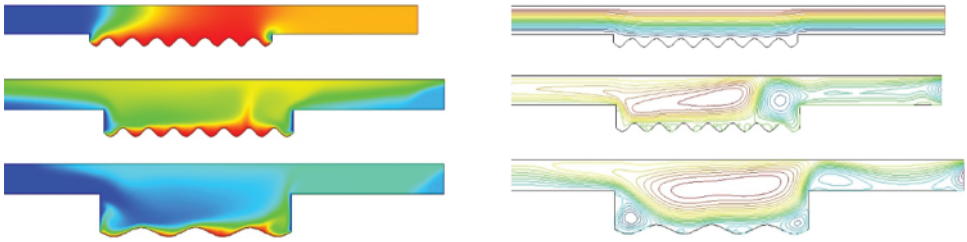

Figure 11: Streamlines and temperature contours at different depths of the cavity and Ri = 10

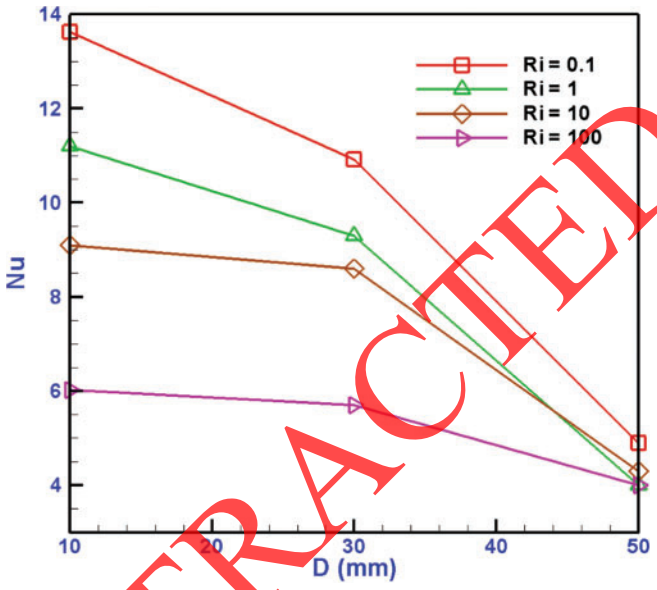

Figure 12: Variations of the average Nusselt number with Richardson number at different depths of the cavity

4 Conclusion

Heat transfer and fluid flow were investigated for the mixed heat transfer in a cavity with a horizontal channel and bottom wavy wall. A second-order upwind scheme was employed for discretizing the convection and diffusion terms. The results obtained through the investigation are summarized below:

- Increasing the depth of the cavity at a constant Richardson number decreases the average Nusselt number on the hot wavy wall.
- Increasing the amplitude of waves of the hot wall at a constant Richardson number increases the heat transfer while increasing the amplitude in the cavity with large depth does not affect the average Nusselt number on the wall significantly.
- At a constant Reynolds number, increasing the wavelength decreases the average Nusselt number. While at any wavelength, increasing the amplitude rises the average Nusselt number of the hot wall.
- By varying the Richardson from 0.1 to 100, the number and shape of the vortices inside the cavity change, and the heat transfer mechanism inside the cavity shifts from forced to free convection.

- Increasing the wave amplitude at low Richardson numbers leads to an increase in the average Nusselt number of the wall, while at high Richardson changes in the amplitude do not alter the average Nusselt number of the wall significantly.
- Increasing the wavelength of the hot wall at the range of Richardson numbers decreases the average Nusselt number.
- The minimum Nusselt number was calculated to be 0.7, while the maximum was 27.09.
- The mean Nusselt number is affected by channel height, and cavity width highly. The effect of wave amplitude on the mean Nusselt number is twice the effect of wavelength on the mean Nusselt number.
- The findings obtained from this study can be used by the HVAC industry to improve the efficiency of their products.

Funding Statement: The authors extend their appreciation to the Deanship of Scientific Research at King Khalid University for funding this work through the Large Groups Project under Grant Number RGP. 2/235/43.

Conflicts of Interest: The authors declare that they have no conflicts of interest to report regarding the present study.

References

[1] M. M. Ali, R. Akhter and M. M. Miah, "Hydromagnetic mixed convective flow in a horizontal channel equipped with Cu-water nanofluid and alternated baffles," *International Journal of Thermofluids*, vol. 12, pp. 100–118, 2021.

[2] L. Yang and K. Du, "A comprehensive review on the natural, forced, and mixed convection of non-newtonian fluids (nanofluids) inside different cavities," *Journal of Thermal Analysis and Calorimetry*, vol. 140, no. 5, pp. 2033–2054, 2020.

[3] D. Qaiser, Z. Zheng and M. Riaz Khan, "Numerical assessment of mixed convection flow of walters-B nanofluid over a stretching surface with newtonian heating and mass transfer," *Thermal Science and Engineering Progress*, vol. 22, pp. 100–106, 2021.

[4] A. N. Sadr, M. Shekaramiz, M. Zarinfar, A. Esmaily, H. Khoshtarash *et al.,* "Simulation of mixed-convection of water and nano-encapsulated phase change material inside a square cavity with a rotating hot cylinder," *Journal of Energy Storage*, vol. 47, pp. 103–110, 2022.

[5] S. Nazari, R. Ellahi, M. M. Sarafraz, M. R. Safaei, A. Asgari *et al.,* "Numerical study on mixed convection of a non-newtonian nanofluid with porous media in a two lid-driven square cavity," *Journal of Thermal Analysis and Calorimetry*, vol. 140, no. 3, pp. 1121–1145, 2020.

[6] A. A. Salamai, E. -S. M. El-kenawy and I. Abdelhameed, "Dynamic voting classifier for risk identification in supply chain 4.0," *Computers, Materials & Continua*, vol. 69, no. 3, pp. 3749–3766, 2021.

[7] M. M. Eid, E. S. M. El-kenawy and A. Ibrahim, "A binary sine cosine-modified whale optimization algorithm for feature selection," in *National Computing Colleges Conf.*, Taif, Saudi Arabia, pp. 1–6, 2021.

[8] R. Taher, M. M. Ahmed, Z. Haddad and C. Abid, "Poiseuille-Rayleigh-bénard mixed convection flow in a channel: Heat transfer and fluid flow patterns," *International Journal of Heat and Mass Transfer*, vol. 180, pp. 121–145, 2021.

[9] P. -Y. Xiong, A. Hamid, K. Iqbal, M. Irfan and M. Khan, "Numerical simulation of mixed convection flow and heat transfer in the lid-driven triangular cavity with different obstacle configurations," *International Communications in Heat and Mass Transfer*, vol. 123, pp. 105–202, 2021.

[10] N. M. Sahraoui, S. Houat and M. El-Ganaoui, "Numerical investigation of low prandtl number effect on mixed convection in a horizontal channel by the lattice boltzmann method," *Heat Transfer*, vol. 49, no. 8, pp. 4528–4542, 2020.

[11] Z. Li, Y. Yao, Q. Wang, J. Cai, Y. Wu *et al.,* "Effect of internal helical-rib roughness on mixed convection flow and heat transfer in heated horizontal pipe flow of supercritical water," *International Journal of Heat and Mass Transfer*, vol. 130, pp. 1272–1287, 2019.
[12] P. Xie and X. Zhang, "A novel method of enhancing convective heat transfer by dynamic controlling rib," *International Communications in Heat and Mass Transfer*, vol. 119, pp. 104–130, 2020.
[13] S. E. Razavi, T. Adibi and H. Hassanpour, "Sensitivity analysis on thermal performance of gas heater with finned and finless tubes using characteristics-based method," *International Journal of Engineering*, vol. 34, no. 6, pp. 1537–1544, 2021.
[14] W. Tang, M. Hatami, J. Zhou and D. Jing, "Natural convection heat transfer in a nanofluid-filled cavity with double sinusoidal wavy walls of various phase deviations," *International Journal of Heat and Mass Transfer*, vol. 115, pp. 430–440, 2017.
[15] S. Yousefzadeh, H. Rajabi, N. Ghajari, M. M. Sarafraz, O. A. Akbari *et al.,* "Numerical investigation of mixed convection heat transfer behavior of nanofluid in a cavity with different heat transfer areas," *Journal of Thermal Analysis and Calorimetry*, vol. 140, no. 6, pp. 2779–2803, 2020.
[16] A. Ullah, Ikramullah, M. M. Selim, T. Abdeljawad, M. Ayaz *et al.,* "A magnetite–water-based nanofluid three-dimensional thin film flow on an inclined rotating surface with non-linear thermal radiations and couple stress effects," *Energies*, vol. 14, pp. 5531–5538, 2021.
[17] S. Khan, M. M. Selim, K. A. Gepreel, A. Ullah, Ikramullah *et al.,* "An analytical investigation of the mixed convective casson fluid flow past a yawed cylinder with heat transfer analysis," *Open Physics*, vol. 19, pp. 341–351, 2021.
[18] I. Ullah, A. Ullah, M. M. Selim, M. I. Khan, Saima *et al.,* "Analytical investigation of magnetized 2D hybrid nanofluid (GO + ZnO + blood) flow through a perforated capillary," *Computer Methods in Biomechanics and Biomedical Engineering*, vol. 1, pp. 1–13, 2022.
[19] Z. Hussain, S. Khan, A. Ullah, Ikramullah, M. Ayaz *et al.,* "Extension of optimal homotopy asymptotic method with use of Daftardar–Jeffery polynomials to Hirota–Satsuma coupled system of Korteweg–de Vries equations," *Open Physics*, vol. 18, pp. 1–14, 2020.
[20] D. Rizk, A. Ullah, Ikramullah, S. Elattar, K. A. M. Alharbi *et al.,* "Impact of the KKL correlation model on the activation of thermal energy for the hybrid nanofluid (GO + ZnO + Water) flow through permeable vertically rotating surface," *Energies*, vol. 12, pp. 13–19, 2022.
[21] S. Khan, M. M. Selim, A. Khan, A. Ullah, T. Abdeljawad *et al.,* "On the analysis of the non-newtonian fluid flow past a stretching/shrinking permeable surface with heat and mass transfer," *Coatings*, vol. 11, pp. 556–565, 2021.
[22] K. A. M. Alharbi, A. Ullah, Ikramullah, N. Fatima, R. Khan *et al.,* "Impact of viscous dissipation and coriolis effects in heat and mass transfer analysis of the 3D non-newtonian fluid flow," *Case Studies in Thermal Engineering*, vol. 37, pp. 289–310, 2022.
[23] S. U. Arifeen, S. Haq, A. Ghafoor, A. Ullah, P. Kumam *et al.,* "Numerical solutions of higher order boundary value problems via wavelet approach," *Advances in Difference Equations*, vol. 347, pp. 34985–96, 2021.
[24] S. Bilal, I. Ali Shah, A. Akgül, M. Taştan Tekin, T. Botmart *et al.,* "A comprehensive mathematical structuring of magnetically effected sutterby fluid flow immersed in dually stratified medium under boundary layer approximations over a linearly stretched surface," *Alexandria Engineering Journal*, vol. 61, pp. 11889–11898, 2022.
[25] S. Bilal and I. A. Shah, "A comprehensive physical insight about thermo physical aspects of carreau fluid flow over a rotated disk of variable thickness by implementing finite difference approach," *Propulsion and Power Research*, vol. 11, pp. 143–153, 2022.
[26] Z. Akbar Qureshi, S. Bilal, U. Khan, A. Akgül, M. Sultana *et al.,* "Mathematical analysis about influence of lorentz force and interfacial nano layers on nanofluids flow through orthogonal porous surfaces with injection of SWCNTs," *Alexandria Engineering Journal*, vol. 61, pp. 12925–12941, 2022.

[27] I. A. Shah, S. Bilal, A. Akgül, M. Taştan Tekin, T. Botmart *et al.,* "On analysis of magnetized viscous fluid flow in permeable channel with single wall carbon nano tubes dispersion by executing nano-layer approach," *Alexandria Engineering Journal*, vol. 61, pp. 11737–11751, 2022.
[28] I. A. Shah, S. Bilal, A. Akgül, M. Omri, J. Bouslimi *et al.,* "Significance of cold cylinder in heat control in power law fluid enclosed in isosceles triangular cavity generated by natural convection: A computational approach," *Alexandria Engineering Journal*, vol. 61, pp. 7277–7290, 2022.
[29] I. A. Shah, S. Bilal, S. Noeiaghdam, U. Fernandez-Gamiz and H. Shahzad, "Thermosolutal natural convection energy transfer in magnetically influenced casson fluid flow in hexagonal enclosure with fillets," *Results in Engineering*, vol. 15, pp. 570–584, 2022.
[30] T. Adibi and S. E. Razavi, "A new characteristic approach for incompressible thermo-flow in cartesian and non-cartesian grids," *International Journal for Numerical Methods in Fluids*, vol. 79, pp. 371–393, 2015.
[31] T. Adibi, S. E. Razavi and O. Adibi, "A characteristic-based numerical simulation of water-titanium dioxide nano-fluid in closed domains," *International Journal of Engineering*, vol. 33, no. 1, pp. 158–163, 2020.
[32] O. Manca, S. Nardini and K. Vafai, "Experimental investigation of mixed convection in a channel with an open cavity," *Experimental Heat Transfer*, vol. 19, no. 1, pp. 53–68, 2006.